

Cite this: *Nanoscale Adv.*, 2020, 2, 1666

Excellent catalysis of Mn_3O_4 nanoparticles on the hydrogen storage properties of MgH_2 : an experimental and theoretical study†

Liuting Zhang,^{‡a} Ze Sun,^{‡a} Zhendong Yao,^{‡c} Lei Yang,^a Nianhua Yan,^a Xiong Lu,^a Beibei Xiao,^a Xinqiao Zhu,^{‡*b} and Lixin Chen,^{‡*c}

Recently, transition metal oxides have been evidenced to be superior catalysts for improving the hydrogen desorption/absorption performance of MgH_2 . In this paper, Mn_3O_4 nanoparticles with a uniform size of around 10 nm were synthesized by a facile chemical method and then introduced to modify the hydrogen storage properties of MgH_2 . With the addition of 10 wt% Mn_3O_4 nanoparticles, the MgH_2 - Mn_3O_4 composite started to release hydrogen at 200 °C and approximately 6.8 wt% H_2 could be released within 8 min at 300 °C. For absorption, the completely dehydrogenated sample took up 5.0 wt% H_2 within 10 min under 3 MPa hydrogen even at 100 °C. Compared with pristine MgH_2 , the activation energy value of absorption for the $\text{MgH}_2 + 10$ wt% Mn_3O_4 composite decreased from 72.5 ± 2.7 to 34.4 ± 0.9 kJ mol⁻¹. The catalytic mechanism of Mn_3O_4 was also explored and discussed with solid evidence from X-ray diffraction (XRD), Transmission Electron Microscope (TEM) and Energy Dispersive X-ray Spectroscopy (EDS) studies. Density functional theory calculations revealed that the Mg-H bonds were elongated and weakened with the doping of Mn_3O_4 . In addition, a cycling test showed that the hydrogen storage capacity and reaction kinetics of MgH_2 - Mn_3O_4 could be favourably preserved in 20 cycles, indicative of promising applications as a solid-state hydrogen storage material in a future hydrogen society.

Received 19th February 2020
Accepted 8th March 2020

DOI: 10.1039/d0na00137f

rsc.li/nanoscale-advances

1. Introduction

Faced with a global energy crisis and environmental issues, the world is crying out for sustainable clean energy sources.¹⁻³ Hydrogen, which can generate electricity *via* fuel cells with nearly no emission of pollutants, is regarded as one of the most promising substitutes for fossil fuels.⁴⁻⁶ In order to store and transfer hydrogen conveniently, efficiently and safely, hydrogen storage materials with a moderate operating temperature, low cost, good dynamics and high hydrogen storage density are urgently required.⁷ Among numerous materials, magnesium hydride (MgH_2) with high mass hydrogen storage capacity (7.76 wt%), good reversibility, low cost and other outstanding performances (LIB anode) has attracted intense attention worldwide.⁸⁻¹¹ Nevertheless, two challenges (stable

thermodynamics and poor kinetics) still need to be conquered before the large scale application of MgH_2 .¹²⁻¹⁴ In the past few decades, extensive research has been conducted to overcome these challenges through diverse methods, such as catalyst doping,¹⁵⁻²⁰ alloying²¹⁻²⁴ and nanotechnology.²⁵⁻²⁷

According to previous reports, transition metals (TMs) and their compounds showed a quite effective influence on improving the hydrogen storage properties of MgH_2 .²⁸⁻³¹ For example, Liu *et al.*³² synthesized a Co@CNT nanocatalyst by carbonizing zeolitic imidazolate framework-67 and doped it into MgH_2 . The experimental results showed that the onset temperature of MgH_2 decreased to 267.8 °C with the addition of Co@CNTs and the dehydrogenation capacity of MgH_2 -Co@CNTs could reach 6.89 wt% at 300 °C within 15 min. For absorption, the MgH_2 -Co@CNTs could absorb 6.15 wt% H_2 at 250 °C within 2 min. Cheng *et al.*³³ found that $\text{Pd}_{30}\text{Ni}_{70}$ /CMK-3 could significantly improve the de/re-hydrogenation performance of MgH_2 at low temperature. About 6 wt% hydrogen could be released below 290 °C and 4 wt% hydrogen could be absorbed at 70 °C under a hydrogen pressure of 3 MPa within 18 000 s. Besides pure metal, metal oxides, which can be easily synthesized, are preferred by scientists to improve the hydrogen storage performance of MgH_2 .³⁴⁻³⁸ Chen *et al.*³⁹ found that a MgH_2 -Co/TiO₂ composite started to desorb hydrogen at about 190 °C with a low apparent activation energy of 77 kJ mol⁻¹. In

^aSchool of Energy and Power, Jiangsu University of Science and Technology, Zhenjiang 212003, China

^bInstitute of Nuclear Physics and Chemistry, China Academy of Engineering Physics, Mianyang, 621999, China. E-mail: zhuxinqiao@zju.edu.cn; Tel: +86 17738406685

^cState Key Laboratory of Silicon Materials, Department of Materials Science and Engineering, Zhejiang University, Hangzhou 310027, China. E-mail: lxchen@zju.edu.cn

† Electronic supplementary information (ESI) available. See DOI: 10.1039/d0na00137f

‡ Liuting Zhang, Ze Sun and Zhendong Yao contributed equally.



addition, the dehydrogenated sample could absorb about 4.24 and 1.0 wt% hydrogen within 10 min at 100 and 50 °C, respectively. Bhatnagar *et al.*⁴⁰ demonstrated that MgH₂ catalyzed by Fe₃O₄@GS offers improved hydrogen storage behaviour. The MgH₂-Fe₃O₄@GS had an onset desorption temperature of about 262 °C and the dehydrogenated sample could absorb 6.20 wt% hydrogen in 2.5 min under 15 atm H₂ pressure at 290 °C. Mustafa *et al.*⁴¹ discovered that a MgH₂-5 wt% CeO₂ sample released about 3.6 wt% hydrogen in 30 min at 320 °C and the dehydrogenated sample could absorb approximately 3.95 wt% hydrogen within 5 min at 320 °C.

Apparently, both transition metals and their oxides can remarkably improve the hydrogen storage properties of MgH₂. In our recent study,⁴² ZrMn₂ was found to strikingly improve the hydrogen storage properties of MgH₂; however, research on the catalytic effect of Mn based compounds on MgH₂ has rarely been reported in the literature. In this work, Mn₃O₄ nanoparticles were successfully synthesized *via* a simple chemical method and adopted to enhance the comprehensive hydrogen storage properties of MgH₂. To our knowledge, no studies have been conducted on doping Mn₃O₄ as a catalyst into MgH₂. Further, the significantly improved hydrogenation and dehydrogenation performance of MgH₂ catalyzed by Mn₃O₄ was systematically studied and the catalytic mechanism was also explored and discussed in detail.

2. Experimental

2.1 Sample preparation

All the chemical reagents were of analytical grade. The nano-Mn₃O₄ powder was prepared by decomposition of Mn(Ac)₂·4H₂O in diethylene glycol (DEG). Firstly, 2.45 g Mn(Ac)₂·4H₂O was dissolved into 100 ml DEG at a temperature of 80 °C. After this, the solution was heated to 160 °C in an oil bath pot and then kept for 8 h. After cooling to room temperature, the suspension was centrifuged and washed with deionized water and ethanol to remove the residual organic solvent. Finally, Mn₃O₄ nanoparticles (nano-Mn₃O₄) can be obtained after vacuum-drying at 70 °C for 10 hours.

MgH₂ was prepared in our laboratory. The magnesium (purity 99.99%) used was purchased from Sinopharm Chemical Reagent. Mg powder was first hydrogenated at 380 °C and under a hydrogen pressure of 65 bar for 2 h. Then the sample was ball-milled at 450 rpm for 5 h and MgH₂ was synthesized by repeating the above hydrogenation treatment. The nano-Mn₃O₄ powder and MgH₂ with mass ratios of 5 : 95, 10 : 90 and 15 : 85 were mixed by ball milling. Ball milling of the above samples was performed on a QM-3SP4 planetary ball mill (Nanjing) at 400 rpm for 2 h under 1 bar of Ar (the ball to material ratio is 40 : 1). To avoid contamination and oxidation, all samples were handled and transferred in an Ar-filled glove box (Mikrouna) where the water/oxygen concentration was less than 0.1 ppm.

2.2 Sample characterization

The phase composition was analyzed by X-ray diffraction (XRD), which was carried out on an X'Pert Pro X-ray diffractometer

(PANalytical, the Netherlands) with Cu K alpha radiation at 40 kV and 40 mA. A special container was used to prevent air and water contamination when samples were transferred and scanned. The morphology of samples was studied using scanning electron microscopy (SEM, Hitachi SU-70) and transmission electron microscopy (TEM, Tecnai G2 F20 STWIN) with energy dispersive spectroscopy (EDS). The hydrogen absorption and desorption results were obtained using Sieverts-type apparatus. Approximately 75 mg sample was heated to 430 °C at a heating rate of 2 °C min⁻¹ in a stainless steel container during testing of the non-isothermal hydrogen desorption properties. Isothermal measurements were performed by quickly heating the sample to the target temperature and then keeping the temperature constant throughout the whole test. In addition, the isothermal absorption performance was measured at various temperatures under a hydrogen pressure of 30 bar while the isothermal desorption performance was tested at different temperatures under a hydrogen pressure below 0.01 bar.

2.3 Theoretical methods

All calculations were carried out within the DMol³ code.^{43,44} The generalized gradient approximation with the Perdew-Burke-Ernzerhof (PBE) functional was used to describe the exchange and correlation effects.⁴⁵ The DFT semi-core pseudopotential (DSPP) core treatment method was used for relativistic effects and replaces the core electrons with an effective potential and introduces a degree of relativistic correction into the core.⁴⁶ The double numerical atomic orbital augmented by a polarization function (DNP) was chosen as the basis set.⁴⁷ To achieve the calculation convergence, a smearing of 0.005 Ha (1 Ha = 27.21 eV) to the orbital occupation was applied. In the geometry structural optimization, the convergence tolerances of energy, maximum force and displacement were 1.0 × 10⁻⁵ Ha, 0.002 Ha Å⁻¹ and 0.005 Å, respectively.

3. Results and discussion

3.1 Characterization of the prepared Mn₃O₄ nanoparticles

The structure and morphologies of the prepared Mn₃O₄ nanoparticles were analysed *via* XRD and TEM measurements, as shown in Fig. 1. Fig. 1a exhibits the TEM image of the Mn₃O₄ sample prepared by the simple chemical method. It can be clearly seen from the picture that the particle size of the as-prepared Mn₃O₄ ranged from 5 nm to 20 nm. Besides, the corresponding SAED image in Fig. 1b reveals that the diffraction rings correspond to the (211)/(220) of Mn₃O₄. In addition, it can be clearly seen from the particle size distribution curve that the size of prepared Mn₃O₄ was mainly concentrated in the range of 7 to 15 nm. The magnified TEM image of the marked part in Fig. 1c is shown in Fig. 1d, where the lattice planes corresponding to the (220) plane of Mn₃O₄ can be observed. The XRD examination result shown in Fig. 1e also indicates that the diffraction peak of Mn₃O₄ (PDF# 24-0734) can be clearly identified. Based on the TEM and XRD results, Mn₃O₄ nanoparticles were successfully synthesized and an outstanding catalytic



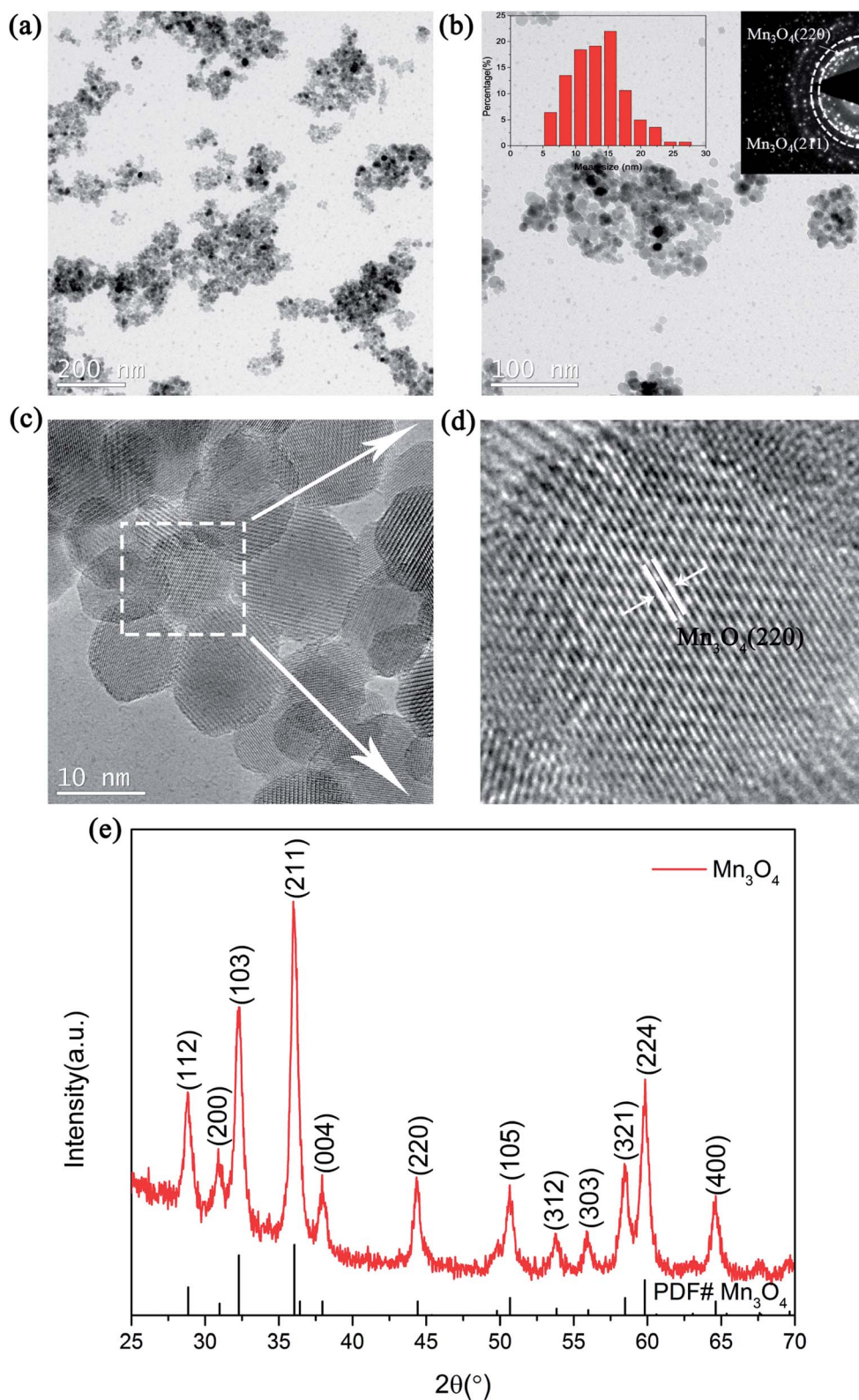


Fig. 1 TEM images (a and c), TEM image with SAED patterns and particle size distribution curve (b), magnified TEM image (d) and XRD pattern (e) of the as-prepared Mn_3O_4 nanoparticles.



effect on improving the hydrogen storage properties of MgH_2 was expected.

3.2 Catalytic effect of the Mn_3O_4 nanoparticles on the hydrogen storage properties of MgH_2

To examine the catalytic effect of Mn_3O_4 on the hydrogen desorption properties of MgH_2 , various amounts of Mn_3O_4 (5, 10 and 15 wt%) were doped into the MgH_2 powders by ball-milling under a 1 bar Ar atmosphere for 2 h. The composites composed of MgH_2 and x wt% Mn_3O_4 nanoparticles ($x = 5, 10$ and 15) were denoted as $\text{MgH}_2 + 5$ wt% Mn_3O_4 , $\text{MgH}_2 + 10$ wt% Mn_3O_4 and $\text{MgH}_2 + 15$ wt% Mn_3O_4 , respectively. All of these milled composites were collected for structural characterization and property tests. Fig. 2a exhibits the XRD patterns of the Mn_3O_4 -doped composites. Clearly, the MgH_2 phase still dominated the XRD profiles and no obvious reacted phases occurred after ball milling. In addition, quite weak peaks of Mg can be seen in this pattern, which could be attributed to the unreacted Mg during synthesis.¹⁵ TPD (Temperature Programmed Desorption) analyses of different amounts of Mn_3O_4 nanoparticle doped MgH_2 samples were also performed. Fig. 2b

depicts the TPD curves of the above three composites and undoped MgH_2 sample, revealing a single step of hydrogen release. It can be observed that the volumetric release curves of $\text{MgH}_2 + \text{Mn}_3\text{O}_4$ composites shifted towards lower temperatures with the increasing added amount of Mn_3O_4 . The as-synthesized MgH_2 began to desorb hydrogen at 340 °C and released about 7.4 wt% hydrogen. With the addition of Mn_3O_4 nanoparticles, the initial desorption temperatures of the $\text{MgH}_2 + 5$ wt% Mn_3O_4 , $\text{MgH}_2 + 10$ wt% Mn_3O_4 and $\text{MgH}_2 + 15$ wt% Mn_3O_4 composites decreased to 230 °C, 200 °C and 200 °C, respectively. To further explore the hydrogen storage properties of the modified MgH_2 systems, isothermal desorption measurements were carried out at 300 °C, as shown in Fig. 2c. The results show that the doping of Mn_3O_4 could significantly improve the hydrogen desorption kinetics of MgH_2 . The $\text{MgH}_2 + 5$ wt% Mn_3O_4 , $\text{MgH}_2 + 10$ wt% Mn_3O_4 and $\text{MgH}_2 + 15$ wt% Mn_3O_4 composites could desorb 6.9 wt%, 6.7 wt% and 6.2 wt% hydrogen in 8 min, while the pure MgH_2 released only 0.038 wt% H_2 in the same duration. From a comprehensive perspective of the dehydrogenation temperature and capacity, the $\text{MgH}_2 + 10$ wt% Mn_3O_4 composite was chosen for further

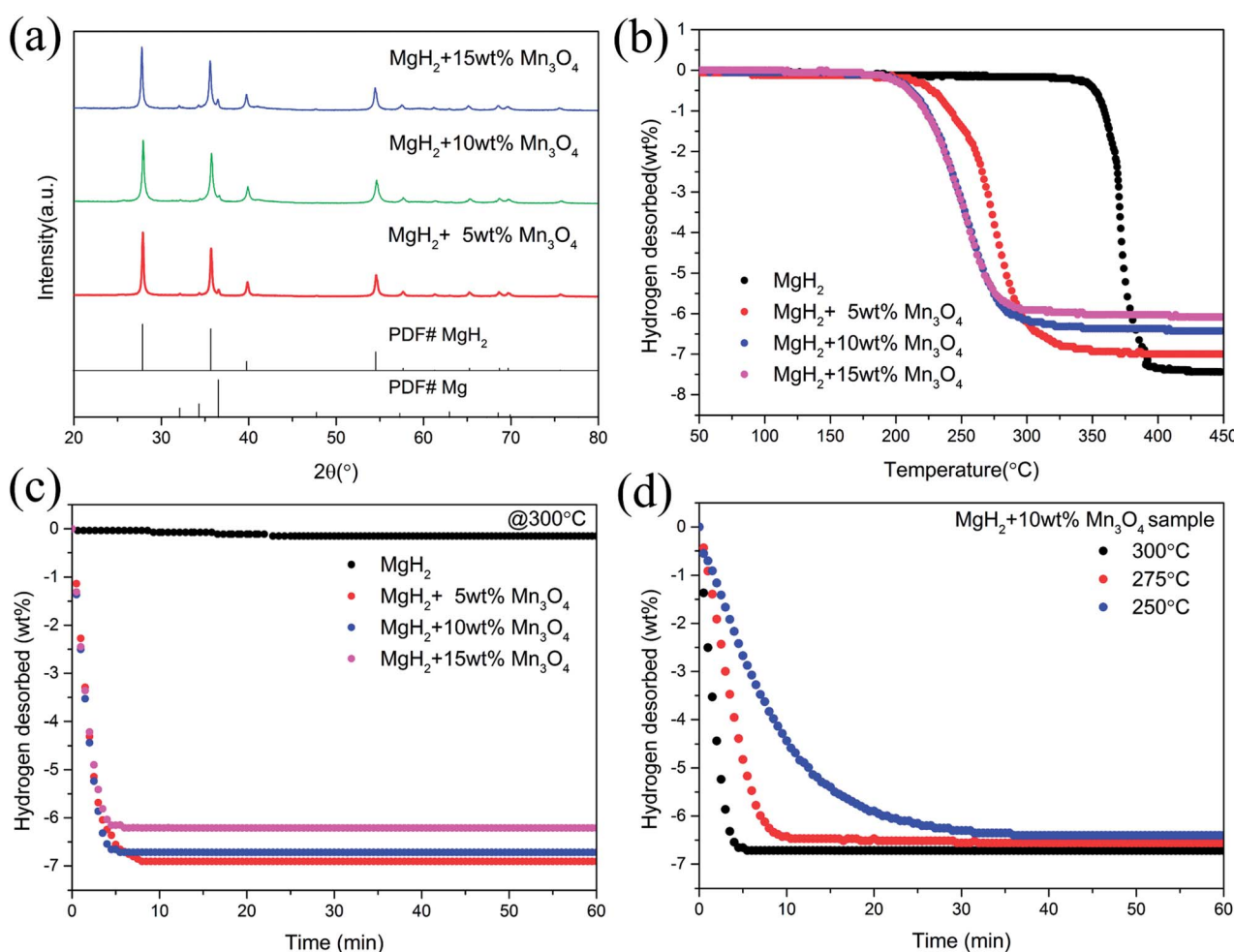


Fig. 2 XRD patterns (a), volumetric release curves (b), and isothermal dehydrogenation curves (c and d) of MgH_2 , $\text{MgH}_2 + 5$ wt% Mn_3O_4 , $\text{MgH}_2 + 10$ wt% Mn_3O_4 , and $\text{MgH}_2 + 15$ wt% Mn_3O_4 samples.



study. Fig. 2d illustrates the isothermal desorption profiles of the $\text{MgH}_2 + 10 \text{ wt\% Mn}_3\text{O}_4$ composite at different temperatures (250, 275 and 300 °C). The composite could release 6.4 wt% hydrogen (nearly 94% of the theoretical hydrogen storage capacity) within 10 min at 275 °C and about 6.3 wt% hydrogen could be desorbed in 30 min even at 250 °C.

Apart from the significantly improved desorption performance, we also focused on the absorption behaviour of the $\text{MgH}_2 + 10 \text{ wt\% Mn}_3\text{O}_4$ composite. The isothermal and non-isothermal hydrogen absorption curves are shown in Fig. 3. Fig. 3a depicts the non-isothermal hydrogenation curves of the prepared MgH_2 and $\text{MgH}_2 + 10 \text{ wt\% Mn}_3\text{O}_4$ samples. The dehydrogenated $\text{MgH}_2 + 10 \text{ wt\% Mn}_3\text{O}_4$ sample started absorbing hydrogen from room temperature, and about 5.4 wt% hydrogen could be taken up before 250 °C. However, the dehydrogenated MgH_2 dilatorily absorbed hydrogen from 183 °C, which was approximately 160 °C higher than that for the dehydrogenated $\text{MgH}_2 + 10 \text{ wt\% Mn}_3\text{O}_4$. Further isothermal absorption measurements of the as-prepared MgH_2 and the $\text{MgH}_2 + 10 \text{ wt\% Mn}_3\text{O}_4$ composite were conducted and the results are presented in Fig. 3b and c. At 50 °C, the

dehydrogenated $\text{MgH}_2 + 10 \text{ wt\% Mn}_3\text{O}_4$ sample exhibited a hydrogen absorption capacity of 2.5 wt% within 20 min. When heated to 75 °C, the hydrogen uptake of the Mn_3O_4 containing sample amounted to 4.1 wt% in 20 min. Within an identical time period, the hydrogen absorption capacity was increased to 5.1 wt% when the temperature was increased to 100 °C. Obviously, the $\text{MgH}_2 + 10 \text{ wt\% Mn}_3\text{O}_4$ sample showed faster hydrogen absorption kinetics than pure MgH_2 (Fig. 3b). Besides, the E_a values of the hydrogen absorption reaction were calculated to further explore the improved hydrogenation kinetics. Fig. 3d reveals the isothermal hydrogenation data of MgH_2 and the $\text{MgH}_2 + 10 \text{ wt\% Mn}_3\text{O}_4$ composite simulated using the Johnson-Mehl-Avrami-Kolmogorov (JMAK) equation,^{48,49} which can be written as:

$$\ln[-\ln(1 - \alpha)] = n \ln k + n \ln t \quad (1)$$

where α is the fraction of Mg transformed into MgH_2 at a particular time, k is an effective kinetic parameter, and n is the Avrami exponent. The values of n and $n \ln k$ obtained by fitting the JMAK plots are shown in Fig. S1.† The E_a values for the

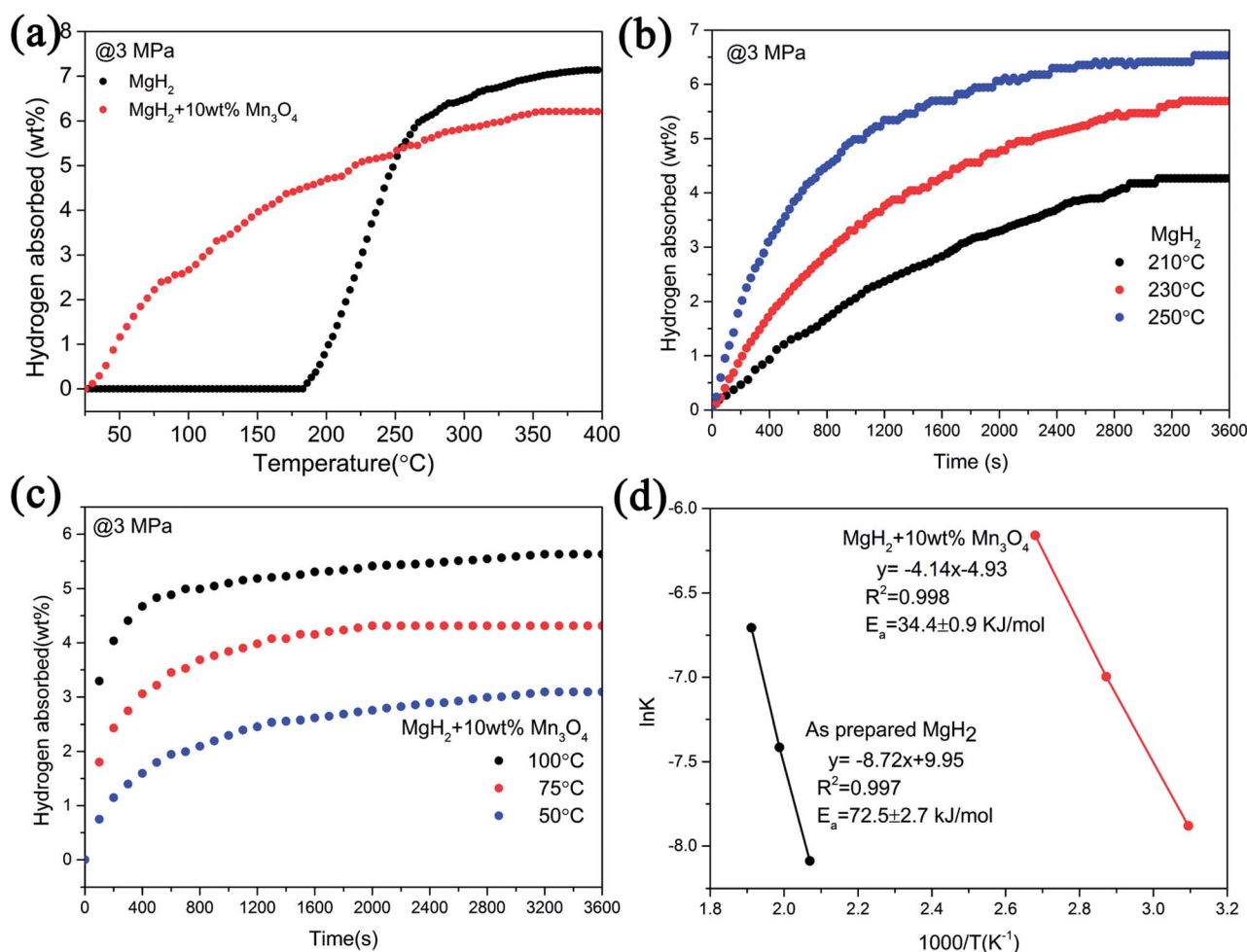


Fig. 3 Non-isothermal hydrogenation curves (a), isothermal hydrogenation curves (b and c) and the corresponding Arrhenius plots (d) of MgH_2 with and without 10 wt% Mn_3O_4 .



hydrogenation reactions were calculated according to the Arrhenius equation:⁵⁰

$$k = A \exp(-E_a/RT) \quad (2)$$

According to the plots in Fig. 3d, the calculated E_a value of the absorption process for the dehydrogenated $\text{MgH}_2 + 10 \text{ wt\% Mn}_3\text{O}_4$ was $34.4 \pm 0.9 \text{ kJ mol}^{-1}$, which was much lower than that of the dehydrogenated MgH_2 ($72.5 \pm 2.7 \text{ kJ mol}^{-1}$) and other MgH_2 -based systems published recently.^{15,16} The E_a for hydrogenation was distinctly decreased by 52.6%, indicating that the energy barrier for the absorption of hydrogen is remarkably reduced due to the addition of Mn_3O_4 , which is reasonably responsible for the enhanced hydrogenation kinetics of the $\text{MgH}_2 + 10 \text{ wt\% Mn}_3\text{O}_4$ composite.

To achieve the practical application of hydrogen storage materials, preserving long-term kinetics is considered one of the key technology indicators. Although favourable hydrogen absorption and desorption properties of Mn_3O_4 doped MgH_2 were evidenced, the cycling performance of the $\text{MgH}_2\text{-Mn}_3\text{O}_4$ composite still needs to be explored. The cycle behaviour of the $\text{MgH}_2 + 10 \text{ wt\% Mn}_3\text{O}_4$ composite was tested at $300 \text{ }^\circ\text{C}$ for 20

cycles. As revealed in Fig. 4, the hydrogen storage capacity of the $\text{MgH}_2 + 10 \text{ wt\% Mn}_3\text{O}_4$ composite reached 6.6 wt% in the first dehydrogenation process. When exposed to a 30 bar hydrogen atmosphere, the dehydrogenated sample could quickly absorb 6.4 wt% H_2 at $300 \text{ }^\circ\text{C}$. After 20 cycles, a high reversible capacity of 6.1 wt% was still maintained, which corresponds to 95.3% of the original capacity. Generally, MgH_2 particles tend to grow and aggregate during pyrolysis, leading to the degradation of cycling performance.^{51,52} In one of our previous studies,¹⁵ the cycling results showed that the capacity of Fe doped MgH_2 was obviously decreased after 20 cycles. It is evident that the hydrogen storage capacity of the $\text{MgH}_2 + 10 \text{ wt\% Mn}_3\text{O}_4$ composite remained stable without significant decline after 20 cycles, revealing remarkable enhancement due to the catalytic activity of Mn_3O_4 nanoparticles.

3.3 De/hydrogenation mechanism

As mentioned above, Mn_3O_4 showed a superior catalytic effect on improving the hydrogen absorption and desorption properties of MgH_2 . For a better understanding of the catalytic mechanism of the Mn_3O_4 modified MgH_2 system, a deeper investigation was conducted. It can be seen in the TEM image (Fig. 5a) that the average size of the $\text{MgH}_2 + 10 \text{ wt\% Mn}_3\text{O}_4$ composite after 20

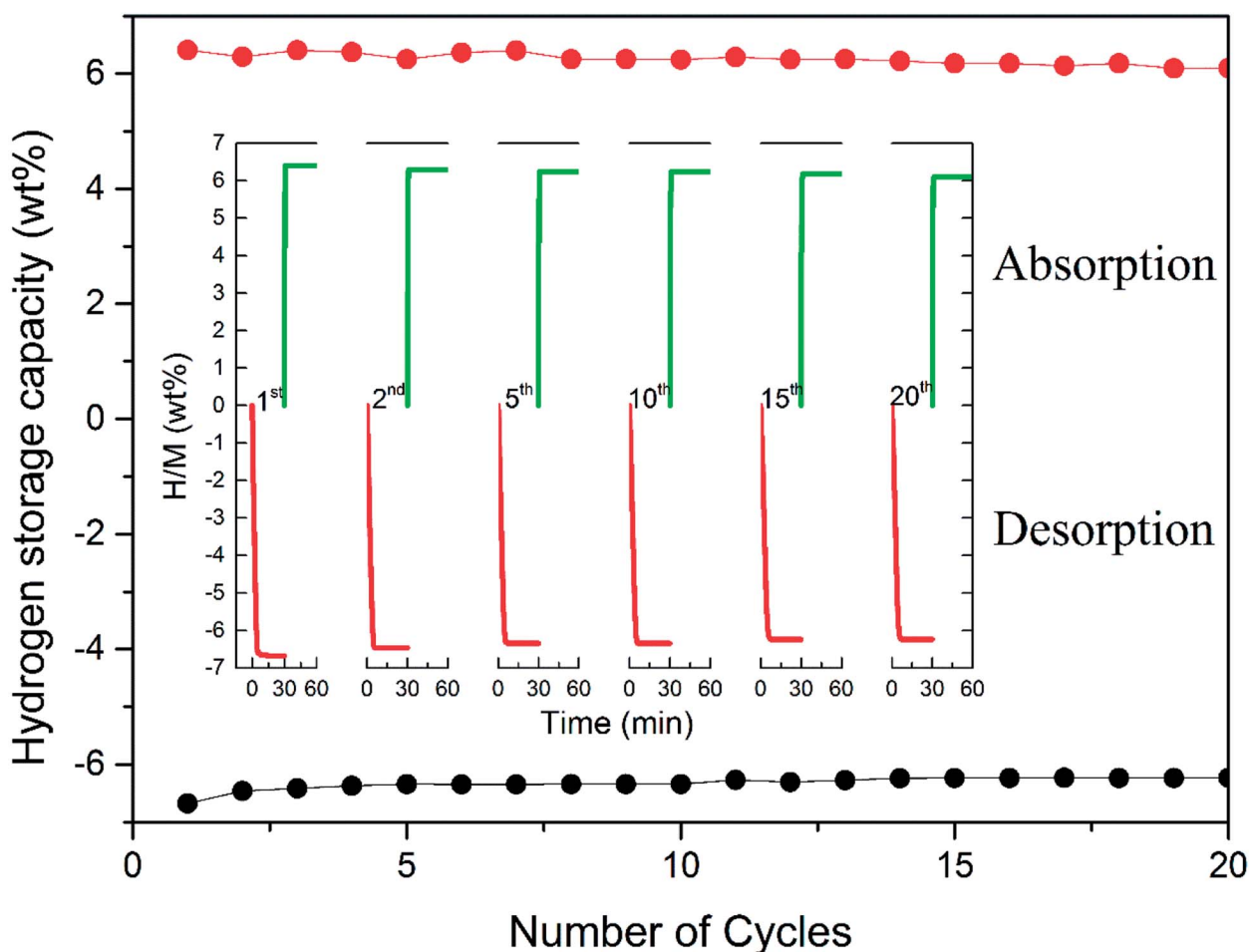


Fig. 4 Non-isothermal dehydrogenation/hydrogenation curves and hydrogen storage capacity of the $\text{MgH}_2 + 10 \text{ wt\% Mn}_3\text{O}_4$ composite.



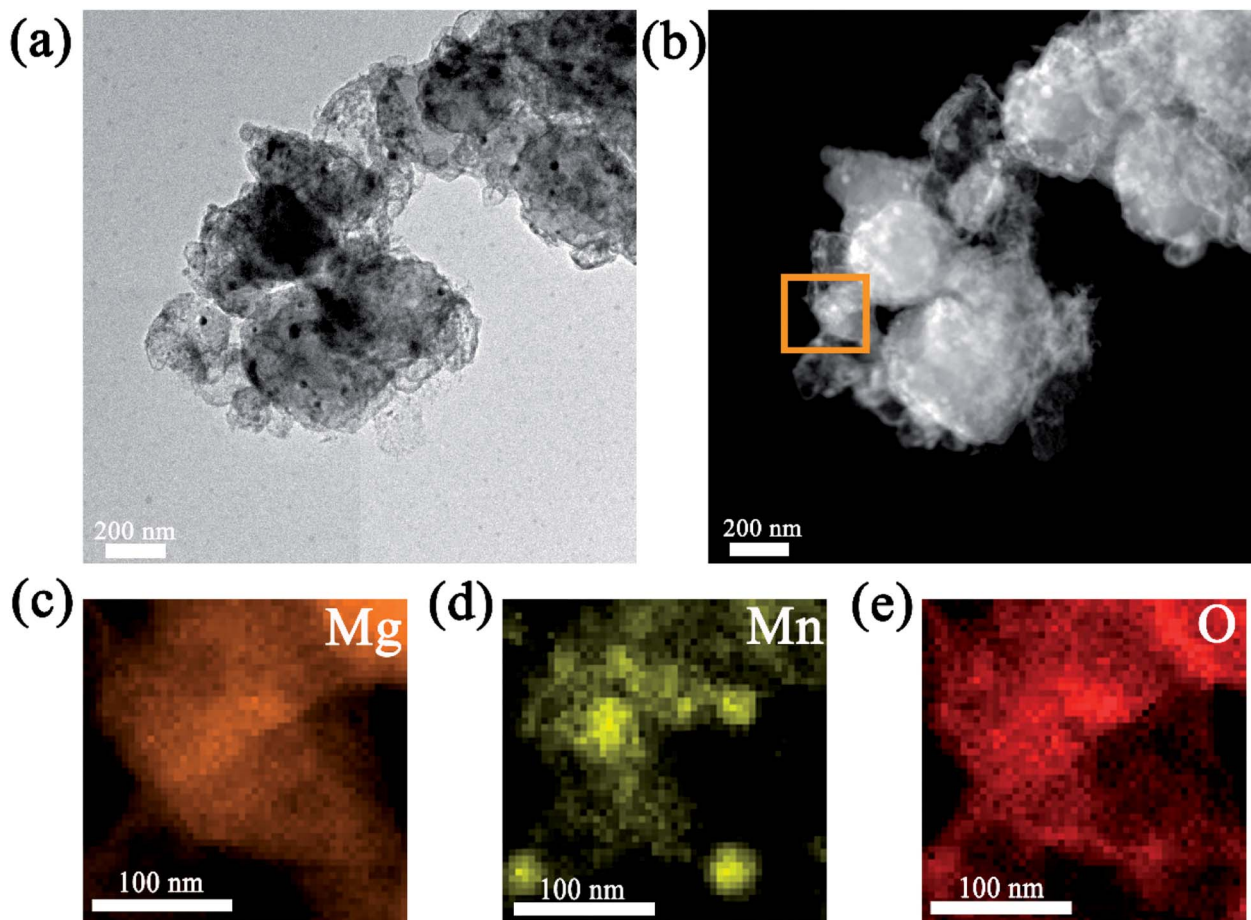


Fig. 5 TEM image (a); STEM-HAADF image (b); corresponding EDS maps (c, d and e) of the $\text{MgH}_2 + 10 \text{ wt\% Mn}_3\text{O}_4$ composite after 20 cycles.

cycles approached 300 nm, which is much smaller than that of ball-milled MgH_2 (over 800 nm) as shown in Fig. S2.† Moreover, the HAADF-STEM image in Fig. 5b shows that numerous bright nanoparticles were homogeneously distributed on the surface of MgH_2 . Corresponding EDS mapping demonstrated that Mn and O covered almost the whole surface of the $\text{MgH}_2 + 10 \text{ wt\% Mn}_3\text{O}_4$ composite after 20 cycles.⁵³

To elucidate the evolution of Mn_3O_4 nanoparticles in the de/hydrogenation process, the $\text{MgH}_2 + 10 \text{ wt\% Mn}_3\text{O}_4$ sample in the ball-milled, dehydrogenated and re-hydrogenated states was collected and examined by XRD measurements (Fig. 6). Although the diffraction peaks of Mn_3O_4 were unclear in the XRD patterns, TEM measurements (Fig. S3†) demonstrated that small particles of Mn_3O_4 can be observed to be evenly distributed on the surface of MgH_2 . Compared with that of pure MgH_2 , the particle size of $\text{MgH}_2 + 10 \text{ wt\% Mn}_3\text{O}_4$ in Fig. S3† was much smaller. Clearly, MgH_2 or Mg still dominated the XRD patterns in Fig. 6 after the doping of Mn_3O_4 . However, it is interesting that Mn and $\text{Mg}_{0.9}\text{Mn}_{0.1}\text{O}$ phases occurred in both the dehydrogenated and rehydrogenated samples, as shown in Fig. 6b and c. In addition, the TEM image (Fig. S4†) reveals that Mn particles were uniformly dispersed on the surface of MgH_2 . It should be pointed out that Mn_3O_4 in contact with Mg can readily form Mn and $\text{Mg}_{0.9}\text{Mn}_{0.1}\text{O}$ under conditions of high

temperature.⁴⁰ The XRD and TEM results indicate that the added Mn_3O_4 nanoparticles were reduced to metallic Mn during the de/hydrogenation process. Therefore, we believe that metallic Mn is the key active catalytic species which enhance the hydrogen release/uptake for MgH_2/Mg .

The impact of Mn metal on the catalytic performance was further investigated by DFT calculations, where the Mn (330) surface was modeled, as shown in the TEM picture. The bond length and the Mulliken population (MP) are described in Fig. 7b. As presented, due to the presence of the Mn support, the Mg–H bonds were dramatically elongated and the average bond length is 2.48 Å, much longer than the pristine one (1.72 Å). Besides, the partial density of states (PDOS) in Fig. 7c shows that the ss-orbital overlap of the Mg–H bond was obviously weakened and the s electrons of Mg and H were mainly distributed at $-5 \sim 0 \text{ eV}$ and $-5 \sim -6 \text{ eV}$, respectively. This reduced orbital interaction corresponds to the faint bond strength, which benefits the de/hydrogenation kinetics.⁵⁴ Therefore, the presence of Mn plays an important role in improving the hydrogen storage properties of the MgH_2 molecule.

Based on the XRD, TEM and calculation results, the whole synthesis and de/hydrogenation process is illustrated in Fig. 8. Mn_3O_4 nanoparticles prepared by a facile chemical method



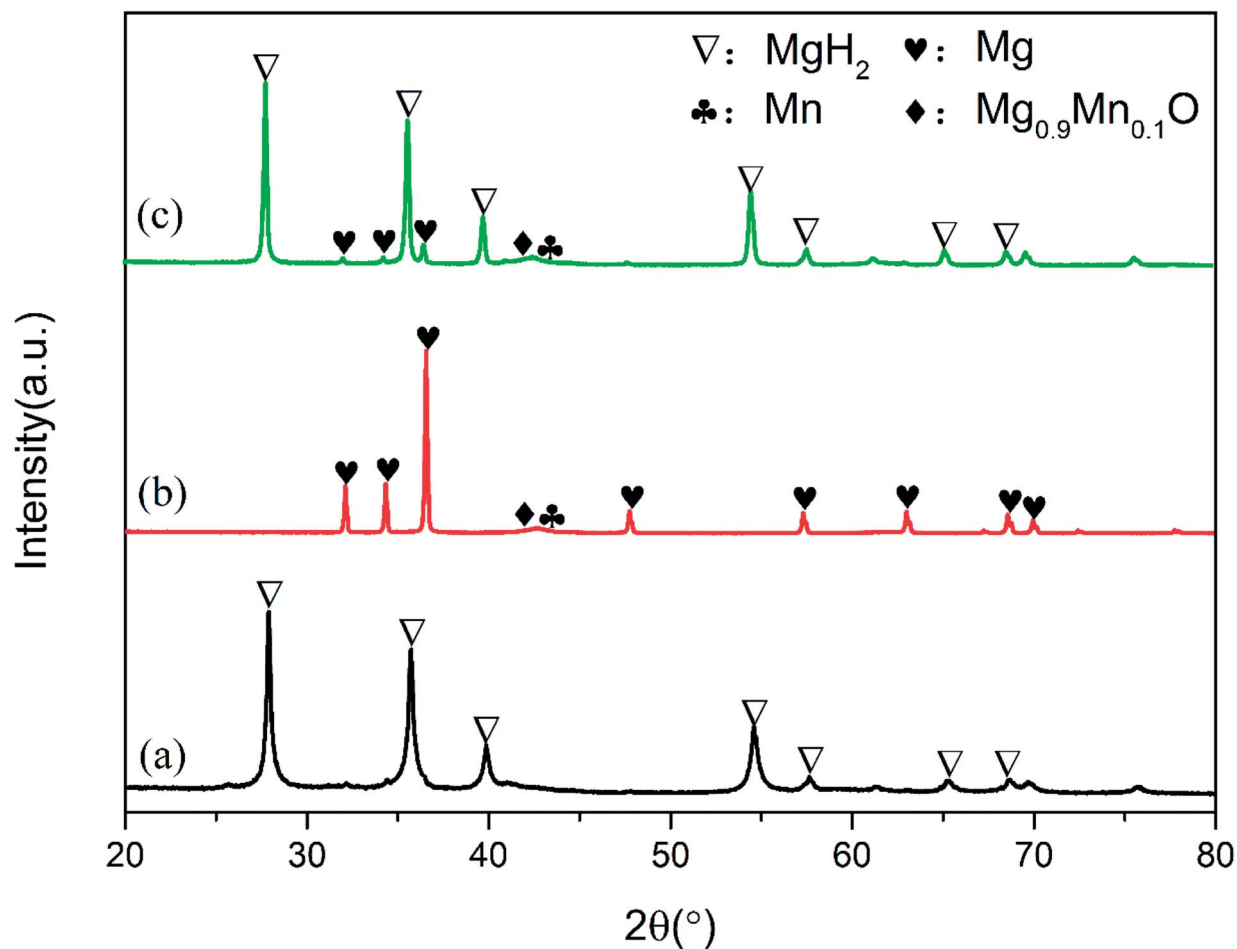


Fig. 6 XRD patterns of ball-milled (a), dehydrogenated (b) and hydrogenated (c) $\text{MgH}_2 + 10 \text{ wt}\% \text{Mn}_3\text{O}_4$ samples.

were evenly decorated on the surface of MgH_2 during ball milling. In the de/hydrogenation process, Mn_3O_4 was reduced to metallic Mn. The Mn “coating”, on one hand, will promote

the fracture of the Mg–H bond in MgH_2 and reduce the de/hydrogenation temperature. On the other hand, it will help to separate the MgH_2 particles and prevent them from growing

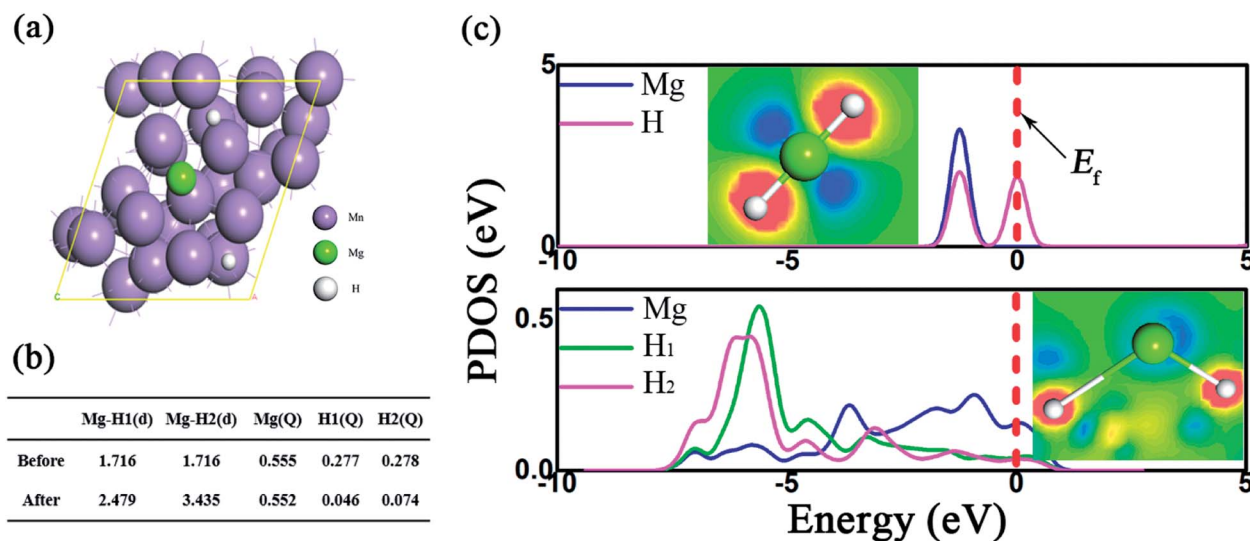


Fig. 7 MgH_2 absorption on the surface of Mn (330). The absorption configuration (a), the bond length, the Mulliken population of Mg–H before and after absorption on the Mn (330) surface (b) and the corresponding partial density of states (c). Inset: the deformation density of MgH_2 where blue or orange denotes the charge depletion or accumulation.



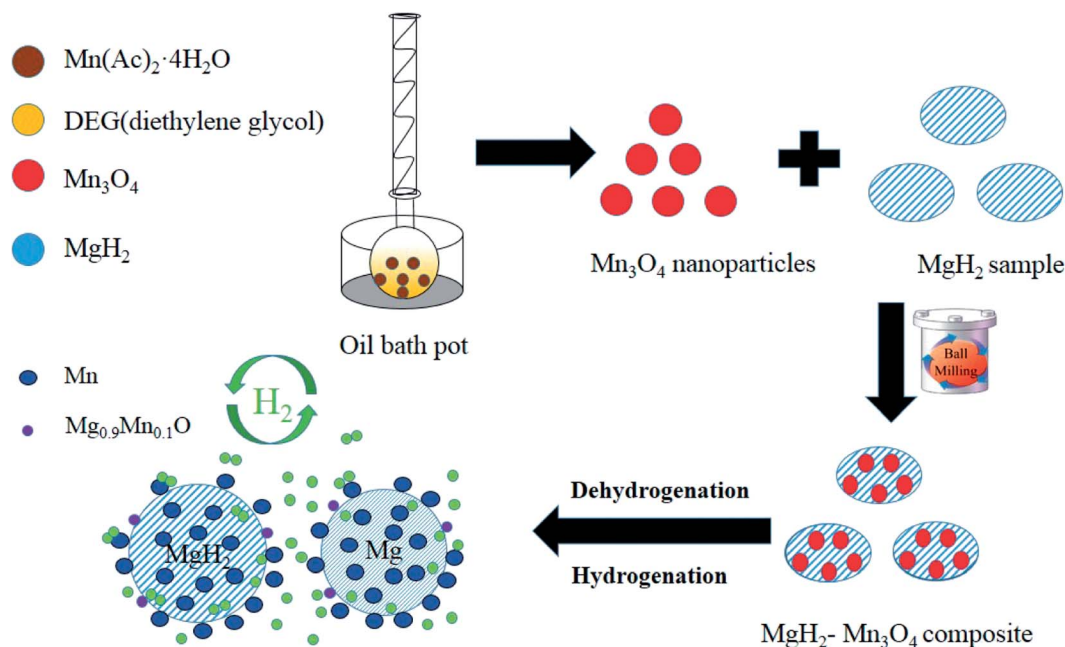


Fig. 8 Schematic summary of the synthesis and de/hydrogenation process in MgH_2 - Mn_3O_4 composites.

and aggregating, thus preserving the stable cycling properties. As a result, the E_a value of the hydrogen absorption reaction was greatly decreased and the hydrogen storage properties of the Mn_3O_4 -doped MgH_2 were significantly enhanced.

4. Conclusion

In summary, Mn_3O_4 nanoparticles around 10 nm were successfully synthesized by a simple chemical method and a series of experiments proved that Mn_3O_4 can remarkably improve the hydrogen storage properties of MgH_2 . During the process of the non-isothermal mode, the $\text{MgH}_2 + 10 \text{ wt}\% \text{ Mn}_3\text{O}_4$ composite released approximately 6.4 wt% hydrogen from 200 °C to 300 °C. Moreover, the $\text{MgH}_2 + 10 \text{ wt}\% \text{ Mn}_3\text{O}_4$ composite desorbed 6.7 wt% hydrogen within 8 min under the isothermal conditions of 300 °C. The dehydrogenated $\text{MgH}_2 + 10 \text{ wt}\% \text{ Mn}_3\text{O}_4$ sample could absorb hydrogen under 3 MPa H_2 pressure even at room temperature, and about 5.4 wt% hydrogen could be charged before 250 °C. The E_a of rehydrogenation of the MgH_2 -10 wt% Mn_3O_4 composite was calculated to be $34.4 \pm 0.9 \text{ kJ mol}^{-1}$. In addition, this sample exhibited favourable cycling stability with no significant fading over 20 cycles. Further XRD, TEM and theoretical calculations revealed that the *in situ* formed Mn weakened the Mg-H bond, and thus greatly promoted the de/hydrogenation reaction and preserved the cycling performance. This study combined experimental results with DFT calculations to investigate the catalytic effect of Mn_3O_4 on improving the hydrogen storage properties of MgH_2 , which will be a good reference for developing a new composite hydrogen storage system.

Conflicts of interest

There are no conflicts to declare.

Acknowledgements

The authors would like to acknowledge the financial support from the National Natural Science Foundation of China (Grant No. 51801078 and 51702300) and the National Science Foundation of Jiangsu Province (Grant No. BK20180986).

References

- 1 T. Sadhasivam, H. Kim, S. Jung, S. Roh, J. Park and H. Jung, *Renewable Sustainable Energy Rev.*, 2017, **72**, 523–534.
- 2 Z. Cao, L. Ouyang, H. Wang, J. Liu, L. Sun, M. Felderhoff and M. Zhu, *Int. J. Hydrogen Energy*, 2016, **41**, 11242–11253.
- 3 Y. Li, X. Zhong, K. Luo and Z. Shao, *J. Mater. Chem. A*, 2019, **7**, 15593–15598.
- 4 J. Zheng, H. Cheng, X. Wang, M. Chen, X. Xiao and L. Chen, *ACS Appl. Energy Mater.*, 2020, DOI: 10.1021/acsaem.0c00134.
- 5 T. Bian, B. Xiao, B. Sun, L. Huang, S. Su, Y. Jiang, J. Xiao, A. Yuan, H. Zhang and D. Yang, *Appl. Catal., B*, 2020, **263**, 118255.
- 6 J. Kim, A. Jun, O. Gwon, S. Yoo, M. Liu, J. Shin, T. H. Lim and G. Kim, *Nano Energy*, 2018, **44**, 121–126.
- 7 N. A. A. Rusman and D. Mahari, *Int. J. Hydrogen Energy*, 2016, **41**, 12108–12126.
- 8 B. Bogdanović, A. Ritter and B. Spliethoff, *Angew. Chem., Int. Ed. Engl.*, 1990, **29**, 223–234.
- 9 I. P. Jain, C. Lal and A. Jain, *Int. J. Hydrogen Energy*, 2010, **35**, 5133–5144.
- 10 X. Peng, H. Wang, R. Hu, L. Ouyang, J. Liu and M. Zhu, *J. Alloys Compd.*, 2017, **711**, 473–479.
- 11 C. Zhou, R. C. Bowman Jr, Z. Z. Fang, J. Lu, L. Xu, P. Sun, H. Liu, H. Wu and Y. Liu, *ACS Appl. Mater. Interfaces*, 2019, **11**, 38868–38879.



- 12 R. Bardhan, A. M. Ruminski, A. Brand and J. J. Urban, *Energy Environ. Sci.*, 2011, **4**, 4882.
- 13 L. Ouyang, X. Yang, M. Zhu, J. Liu, H. Dong, D. Sun, J. Zou and X. Yao, *J. Phys. Chem. C*, 2014, **118**, 7808–7820.
- 14 P. Rizo-Acosta, F. Cuevas and M. Latroche, *J. Mater. Chem. A*, 2019, **7**, 23064–23075.
- 15 L. Zhang, L. Ji, Z. Yao, N. Yan, Z. Sun, X. Yang, X. Zhu, S. Hu and L. Chen, *Int. J. Hydrogen Energy*, 2019, **44**, 21955–21964.
- 16 L. Zhang, Z. Cai, X. Zhu, Z. Yao, Z. Sun, L. Ji, N. Yan, B. Xiao and L. Chen, *J. Alloys Compd.*, 2019, **805**, 295–302.
- 17 W. Su, Y. Zhu, J. Zhang, Y. Liu, Y. Yang, Q. Mao and L. Li, *J. Alloys Compd.*, 2016, **669**, 8–18.
- 18 G. Xia, Y. Tan, X. Chen, D. Sun, Z. Guo, H. Liu, L. Ouyang, M. Zhu and X. Yu, *Adv. Mater.*, 2015, **27**, 5981–5988.
- 19 S. Gao, X. Wang, H. Liu, T. He, Y. Wang, S. Li and M. Yan, *J. Power Sources*, 2019, **438**, 227006.
- 20 S. Gao, H. Liu, L. Xu, S. Li, X. Wang and M. Yan, *J. Alloys Compd.*, 2018, **735**, 635–642.
- 21 L. Ji, L. Zhang, X. Yang, X. Zhu and L. X. Chen, *Dalton Trans.*, 2020, DOI: 10.1039/d0dt00230e.
- 22 M. Bououdina and Z. X. Guo, *J. Alloys Compd.*, 2002, **336**, 222–231.
- 23 B. Liao, Y. Lei, L. Chen, G. Lu, H. Pan and Q. Wang, *J. Power Sources*, 2004, **129**, 358–367.
- 24 N. A. Ali, N. H. Idris, M. F. M. Din, M. S. Yahya and M. Ismail, *J. Alloys Compd.*, 2019, **796**, 279–286.
- 25 T. K. Nielsen, K. Manickam, M. Hirscher, F. Besenbacher and T. R. Jensen, *ACS Nano*, 2009, **3**, 3521–3528.
- 26 G. Chen, Y. Zhang, J. Chen, X. Guo, Y. Zhu and L. Li, *Nanotechnology*, 2018, **29**, 265705.
- 27 Z. Ma, J. Zhang, Y. Zhu, H. Lin, Y. Liu, Y. Zhang, D. Zhu and L. Li, *ACS Appl. Energy Mater.*, 2018, **1**, 1158–1165.
- 28 Y. Jia, L. Cheng, N. Pan, J. Zou, G. Max Lu and X. Yao, *Adv. Energy Mater.*, 2011, **1**, 387–393.
- 29 M. P. Pitt, M. Paskevicius, C. J. Webb, D. A. Sheppard, C. E. Buckley and E. M. Gray, *Int. J. Hydrogen Energy*, 2012, **37**, 4227–4237.
- 30 J. Cui, J. Liu, H. Wang, L. Ouyang, D. Sun, M. Zhu and X. Yao, *J. Mater. Chem. A*, 2014, **2**, 9645–9655.
- 31 Z. Wang, X. Zhang, Z. Ren, Y. Liu, J. Hu, H. Li, M. Gao, H. Pan and Y. Liu, *J. Mater. Chem. A*, 2019, **7**, 14244–14252.
- 32 M. Liu, X. Xiao, S. Zhao, S. Saremi-Yarahmadi, M. Chen, J. Zheng, S. Li and L. Chen, *Int. J. Hydrogen Energy*, 2019, **44**, 1059–1069.
- 33 H. Cheng, G. Chen, Y. Zhang, Y. Zhu and L. Li, *Int. J. Hydrogen Energy*, 2019, **44**, 10777–10787.
- 34 M. Mehta, N. Kodan, S. Kumar, A. Kaushal, L. Mayrhofer, M. Walter, M. Moseler, A. Dey, S. Krishnamurthy, S. Basu and A. P. Singh, *J. Mater. Chem. A*, 2016, **4**, 2670–2681.
- 35 S. Kumar, Y. Kojima and G. K. Dey, *Int. J. Hydrogen Energy*, 2018, **43**, 809–816.
- 36 H. Chen, P. Liu, J. Li, Y. Wang, C. She, J. Liu, L. Zhang, Q. Yang, S. Zhou and X. Feng, *ACS Appl. Mater. Interfaces*, 2019, **11**, 31009–31017.
- 37 Z. Ma, J. Liu, Y. Zhu, Y. Zhao, H. Lin, Y. Zhang, H. Li, J. Zhang, Y. Liu, W. Gao, S. Li and L. Li, *J. Alloys Compd.*, 2020, **822**, 153553.
- 38 H. Lin, J. Tang, Q. Yu, H. Wang, L. Ouyang, Y. Zhao, J. Liu, W. Wang and M. Zhu, *Nano Energy*, 2014, **8**, 80–87.
- 39 M. Chen, X. Xiao, M. Zhang, J. Zheng, M. Liu, X. Wang, L. Jiang and L. Chen, *Int. J. Hydrogen Energy*, 2019, **44**, 15100–15109.
- 40 A. Bhatnagar, S. K. Pandey, A. K. Vishwakarma, S. Singh, V. Shukla, P. K. Soni, M. A. Shaz and O. N. Srivastava, *J. Mater. Chem. A*, 2016, **4**, 14761–14772.
- 41 N. S. Mustafa and M. Ismail, *J. Alloys Compd.*, 2017, **695**, 2532–2538.
- 42 L. Zhang, Z. Cai, Z. Yao, L. Ji, Z. Sun, N. Yan, B. Zhang, B. Xiao, J. Du, X. Zhu and L. Chen, *J. Mater. Chem. A*, 2019, **7**, 5626–5634.
- 43 G. Kresse and J. Furthmuller, *Comput. Mater. Sci.*, 1996, **6**, 15–50.
- 44 B. Xiao, H. Liu, L. Yang, E. Song, X. Jiang and Q. Jiang, *ACS Appl. Energy Mater.*, 2020, **3**, 260–267.
- 45 K. B. J. P. Perdew and M. Ernzerhof, *Phys. Rev. Lett.*, 1996, **77**, 3865–3868.
- 46 B. Xiao, H. Liu, X. Jiang, Z. Yu and Q. Jiang, *RSC Adv.*, 2017, **7**, 54332–54340.
- 47 W. Tang, E. Sanville and G. Henkelman, *J. Phys.: Condens. Matter*, 2009, **21**, 084204.
- 48 M. Avrami, *J. Chem. Phys.*, 1939, **7**, 1103–1112.
- 49 M. Liu, S. Zhao, X. Xiao, M. Chen, C. Sun, Z. Yao, Z. Hu and L. Chen, *Nano Energy*, 2019, **61**, 540–549.
- 50 F. Jensen, *Qual. Reliab. Eng. Int.*, 1985, **1**, 13–17.
- 51 B. Paik, I. P. Jones, A. Walton, V. Mann, D. Book and I. R. Harris, *J. Alloys Compd.*, 2010, **492**, 515–520.
- 52 J. Chen, G. Xia, Z. Guo, Z. Huang, H. Liu and X. Yu, *J. Mater. Chem. A*, 2015, **3**, 15843–15848.
- 53 L. Zhang, Z. Sun, Z. Cai, N. Yan, X. Lu, X. Zhu and L. Chen, *Appl. Surf. Sci.*, 2020, **504**, 144465.
- 54 X. Zhang, Z. Leng, M. Gao, J. Hu, F. Du, J. Yao, H. Pan and Y. Liu, *J. Power Sources*, 2018, **398**, 183–192.

